ELSEVIER

Polymer 41 (2000) 867–874

polymer

Microscopic visualization on crystalline morphologies of thin films for poly[(*R*)-3-hydroxybutyric acid] and its copolymer

H. Abe[a,*], Y. Kikkawa[b], T. Iwata[a], H. Aoki[b], T. Akehata[b], Y. Doi[a]

[a]*Polymer Chemistry Laboratory, The Institute of Physical and Chemical Research (RIKEN), Hirosawa, Wako-shi, Saitama 351-0198, Japan*
[b]*Department of Industrial Chemistry, Science University of Tokyo, 1-3, Kagurazaka, Shinjuku-ku, Tokyo 162-8601, Japan*

Received 17 February 1999; accepted 15 March 1999

Abstract

Thin films with average layer thickness 100 nm of poly[(*R*)-3-hydroxybutyric acid] (P[(*R*)-3HB]) and poly[(*R*)-3-hydroxybutyric acid-*co*-10 mol% 6-hydroxyhexanoic acid] were isothermally crystallized at a given crystallization temperature after melting at 200°C. The spherulitic and lamellar morphologies of polyester thin films were investigated by means of optical microscopy, transmission electron microscopy and atomic force microscopy. After isothermal crystallization, the uniform two-dimensional spherulites which have the stacking texture of flat-on lamellae were developed throughout both polyester thin films. Each flat-on crystal gave a well-resolved electron diffractogram, and all electron diffractograms were identical. Accordingly, the 6-hydroxyhexanoic acid units were rejected from the tightly packed region of lamellar crystals. Both the lamellar periodicity and lamellar width of polyester thin films increased with a rise in the crystallization temperature. At the growth front of crystalline lamellae, microfibril crystals with 30–50 nm width were present. The enzymatic hydrolysis of thin films was carried out at 25°C using an aqueous solution of PHB depolymerase from *Alcaligenes faecalis*. After enzymatic degradation, the jagged texture along the crystal long-axis could be observed at the ends of crystalline lamellae on the surface of the thin films. These observations suggest that the lamellar crystals of P[(*R*)-3HB] is composed of both tight molecular packing regions of microfibril crystals and loose molecular packing boundary regions.

Keywords: Poly[(*R*)-3-hydroxybutyric acid]; Thin film; Lamellar morphology

1. Introduction

Poly[(*R*)-3-hydroxybutyric acid] (P[(*R*)-3HB]) and its copolymers, poly(hydroxyalkanoic acid)s (PHA), are biodegradable thermoplastics produced from renewable carbon sources by a number of bacteria [1–3]. These microbial PHA polymers have attracted much attention as environmentally degradable thermoplastics to be used for a wide range of agricultural, marine and medical applications [1]. A remarkable characteristic of PHAs is their biodegradability in various environments [1,2]. A number of micro-organisms such as bacteria and fungi in environments excrete PHB depolymerases to hydrolyze the solid PHA into water-soluble oligomers and monomer, and they utilize the resulting products as nutrients within cells. Aerobic and anaerobic PHA-degrading micro-organisms have been isolated from various ecosystems, and the properties of their extracellular PHB depolymerases have been studied [4–6].

To elucidate the mechanism of enzymatic hydrolysis of PHA materials with PHB depolymerases, the enzymatic reaction has been investigated using films and single crystals of PHA. The effects of chemical structure of second monomer units and copolymer compositions on the rate of enzymatic erosion have been examined through the enzymatic degradation of the solvent-cast films of various PHA copolymers in the presence of PHB depolymerase from *Alcaligenes faecalis* [7–11]. The rate of enzymatic erosion on the solvent-cast PHA films increased markedly with an increase in the fraction of second monomer units up to 10–20 mol% to reach a maximum value followed by a decrease in the erosion rate.

The melt-crystallized films of P[(*R*)-3HB] [12–14] and its copolymers [8–11] exhibit large banded spherulites, and the spherulitic morphology and degree of crystallinity are dependent on the crystallization conditions. Kumagai et al. [14] reported that the rate of enzymatic hydrolysis of melt-crystallized P[(*R*)-3HB] film by PHB depolymerase from *A. faecalis* decreased with an increase in the crystallinity of P[(*R*)-3HB] film, while the size of spherulites did not have an effect on the rate of hydrolysis. Tomasi et al. [15] reported that the rate of enzymatic erosion of melt-crystallized P[(*R*)-3HB] films with PHB depolymerase from

* Corresponding author. Tel.: + 81-48-467-9404; fax: +81-48-462-4667.
E-mail address: habe@postman.riken.go.jp (H. Abe)

0032-3861/00/$ - see front matter
PII: S0032-3861(99)00231-1

Pseudomonas lemoignei decreased with an increase in the average size of P[(*R*)-3HB] crystals. Koyama and Doi [16] studied the enzymatic degradabilities of melt-crystallized films of various PHA copolymers by PHB depolymerase from *A. faecalis* and reported that the erosion rates for poly[(*R*)-3-hydroxybutyric acid-co-7 mol% (*R*)-3-hydroxypentanoic acid] films were several times higher than the rates of P[(*R*)-3HB] homopolymer films with the same degree of crystallinity. Recently, we investigated the lamellar crystal structures for melt-crystallized films of copolymers of (*R*)-3HB with different hydroxyalkanoic acids by using a small-angle X-ray scattering technique [17]. In addition, the rates of enzymatic erosion of melt-crystallized PHA films were measured in the presence of PHB depolymerase from *A. faecalis*, and the enzymatic erosion rate of crystalline phase was found to decrease markedly with an increase in the lamellar thickness.

Several groups [18–22] have studied the enzymatic degradation of monolamellar single crystals of P[(*R*)-3HB] with PHB depolymerases from bacteria and fungi, and all of them reported that the single crystals were enzymatically hydrolyzed preferentially at the disordered chain-packing regions of crystal edges rather than the chain-folding surfaces of single crystals. Furthermore, it was revealed that the crystalline lamellae have splintered longitudinally into a needle-like morphology along their crystallographic *a*-axis of single crystals.

These reported results indicate that the enzymatic degradation of PHA is strongly affected by the structure of lamellar crystal, and prompted us to investigate the lamellar crystal morphologies of PHA by atomic level. The single crystals which have clear, uniform and well-defined structure are the monolamellar system. In contrast, the bulk materials such as films and plates are the multi-lamellar systems which aggregate the multi-oriented lamellar crystals. Accordingly, in this paper, we prepare the melt-crystallized PHA thin films with a layer thickness of 100 nm from P[(*R*)-3HB] homopolymer and a random copolymer of 90 mol% (*R*)-3HB and 10 mol% 6-hydroxyhexanoic acid (6HH) units in which the lamellar crystals grow two-dimensionally (hedritic growth). The spherulitic and lamellar morphologies of PHA thin films are characterized by using optical microscopy, transmission electron microscopy (TEM) and atomic force microscopy (AFM).

2. Experimental

2.1. Materials

Poly[(*R*)-3-hydroxybutyric acid] (P[(*R*)-3HB]) was prepared by the microbial synthetic methods [23]. Number-average molecular weight (M_n), polydispersity (M_w/M_n) and glass transition temperature (T_g) of P[(*R*)-3HB] homopolymer were 281 000, 2.3 and 4°C, respectively. Poly[(*R*)-3-hydroxybutyric acid-*co*-10 mol% 6-hydroxyhexanoic acid] (P[(*R*)-3HB-*co*-10 mol% 6HH]) was synthesized by the ring-opening copolymerization of (*R*)-β-butyrolactone (e.e. 92%) with ϵ-caprolactone in the presence of tin-based catalyst [10]. The values of M_n, M_w/M_n and T_g of P[(*R*)-3HB-*co*-10 mol% 6HH] were 107 000, 1.7 and −5°C, respectively. By analysis of the ^{13}C nuclear magnetic resonance spectra of P[(*R*)-3HB-*co*-10 mol% 6HH], the sequence distributions of (*R*)-3HB and 6HH units was found to be statistically random [10].

2.2. Preparation of melt-crystallized thin films

Thin films of 100 nm thickness of P[(*R*)-3HB] and P[(*R*)-3HB-*co*-10 mol% 6HH] were initially prepared by solvent-cast technique from chloroform solutions of polymers. Droplet of 10 μl of polymer solution (1.0% (w/v)) was placed on one substrate (substrate dimensions: 18 × 18 mm) and interposed with the other substrate to spread the solution. After then, the two substrates were slid over each other, and the thin layer of polyester was formed on the surface of the substrate. The thin layers on the substrate were heated on the hot-stage (Linkam LK-600PM) from room temperature to 200°C at a rate of 30°C min^{-1}. Samples were maintained at 200°C for 30 s, and then the temperature was rapidly lowered to a given crystallization temperature (T_c) of 30–120°C. The samples were crystallized isothermally at a given T_c periodically. Either cover-glass or carbon-coated mica was used as the base substrate.

2.3. Enzymatic degradation of thin films

The extracellular PHB depolymerase from *Alcaligenes faecalis* T1 was purified to electrophoretic homogeneity by the method of Shirakura et al. [24]. A droplet of 50 μl of 0.1 M potassium phosphate buffer (pH 7.4) containing PHB depolymerase (1.0 μg ml^{-1}) was placed on the thin film surface. The enzymatic degradation of thin films by PHB depolymerase was carried out at 25°C. The enzyme solution was removed from the thin film surface after reaction for a specific time, and then the thin film was washed with distilled water, and dried to constant weight in vacuo before analysis.

2.4. Analytical procedures

Spherulitic morphologies of melt-crystallized thin films were observed with an optical microscope (Nikon OPTIPHOTO-2) equipped with crossed polarizers.

Transmission electron microscopy (TEM) was performed with a JEM-2000FX II electron microscope operated at an acceleration voltage of 200 kV for electron diffraction and 120 kV for the imaging of shadowed crystals. Electron diffraction diagrams and images were recorded on Kodak SO-163 and 4489 films, respectively. The polyester–carbon thin films prepared on the carbon-coated mica surface were relieved on a water surface, picked up on a copper grid, allowed to dry and then shadowed with a Pt–Pd alloy for

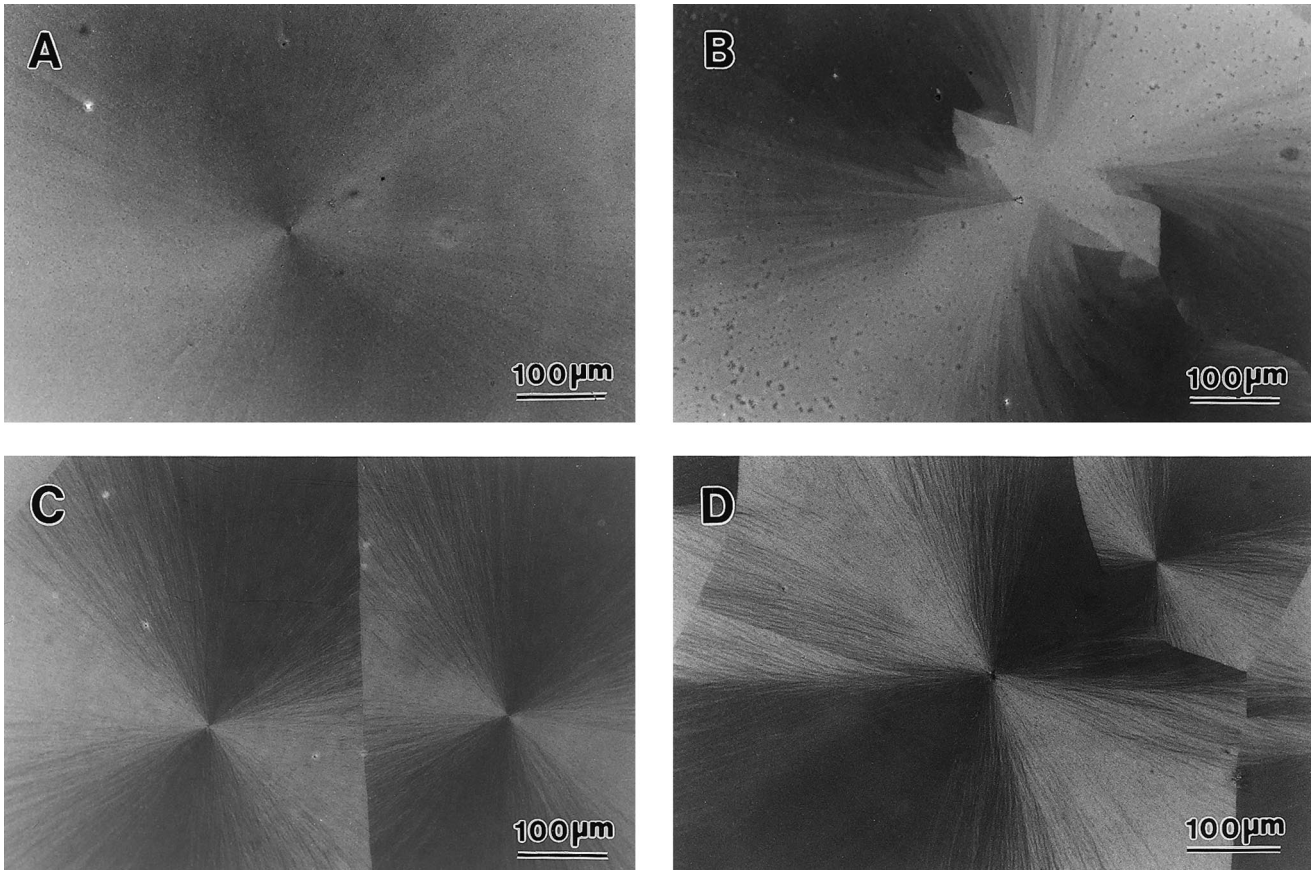

Fig. 1. Optical micrographs of P[(*R*)-3HB] thin films crystallized at 60°C (A) and 120°C (B), and of P[(*R*)-3HB-*co*-10 mol% 6HH] thin films crystallized at 50°C (C) and 110°C (D).

images. For electron diffraction purposes, the thin films were only allowed to dry. The thin films were shadowed with evaporated gold (Au) for calibration.

Atomic force microscopy (AFM) was performed with a SPI3700/SPA300 (Seiko Instruments Inc.). Pyramid-like silicon tips, mounted on 200 μm long microcantilevers with spring constants of 14 N m^{-1} were applied for the dynamic force mode experiments. Simultaneous registration was performed for height and deflection images.

3. Results and discussion

Thin films of P[(*R*)-3HB] and P[(*R*)-3HB-*co*-10 mol% 6HH] were firstly prepared by solvent-cast technique from chloroform solutions of polymers (see Section 2). For measurement of layer thickness, the polymer thin layer was separated from substrate by immersing into water and characterized on the basis of AFM. Average thickness of polyester thin films could be regulated in the range 50–200 nm with reproducibility by varying the concentration of polymers in chloroform from 0.5 to 2.0% (w/v).

Thin films, about 100 nm thick, of P[(*R*)-3HB] and P[(*R*)-3HB-*co*-10 mol% 6HH] were crystallized isothermally at a given crystallization temperature from the melt at 200°C and viewed under cross-polars in the optical microscope. Fig. 1 shows the typical optical micrographs for thin films of P[(*R*)-3HB] and P[(*R*)-3HB-*co*-10 mol% 6HH] isothermally crystallized at various temperatures on glass substrates. For all thin films, the uniform spherulites were developed throughout the thin film. The mean spherulite size increased with a rise in the crystallization temperature due to a decrease in the nucleation rate. It has been reported that the P[(*R*)-3HB] spherulites in melt-crystallized thick films showed both the Maltese-cross and the banded-ring patterns corresponding to an optical birefringence for P[(*R*)-3HB] crystals [12]. The Maltese-cross pattern originates from a parallel or perpendicular crystal axis with respect to the polarization direction. The banded morphology of spherulites is known to arise from the difference of orientation of crystalline axis due to periodical twisting of lamellar crystals. In this study, the spherulites grown in thin films displayed a characteristic Maltese-cross pattern, while the banded texture was not detected. This result suggests that the lamellar crystal grows two-dimensionally along to the spherulite radius without lamellar twisting. Similar spherulitic morphologies were observed in the thin films prepared on the carbon-coated mica substrates, indicating that the effect of based substrate on the crystal morphologies hardly exists.

Lamellar features in thin films were characterized by using transmission electron microscope. Typical electron

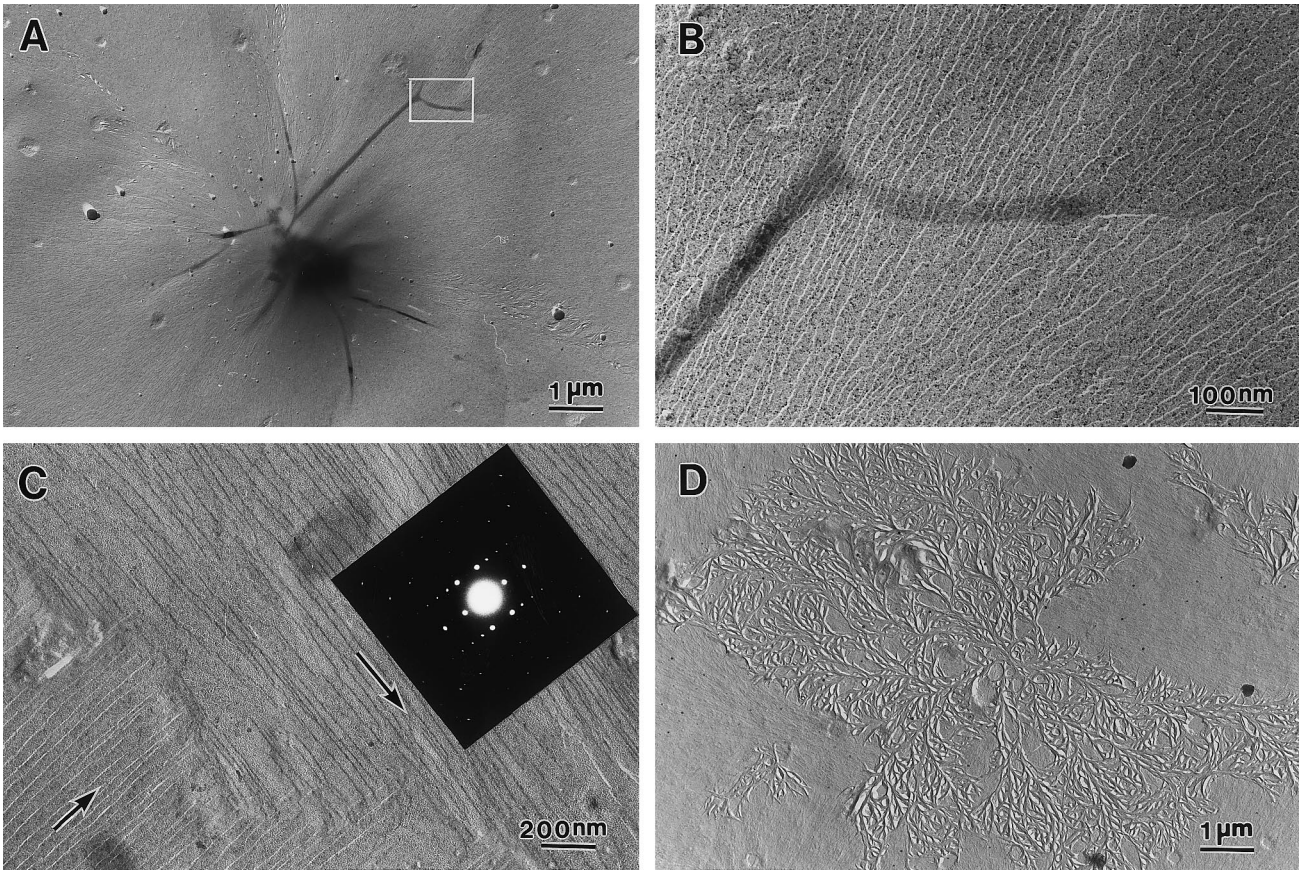

Fig. 2. Electron micrographs of P[(*R*)-3HB] thin films crystallized at 60°C (A and B) and 120°C (C and D). (A) Low magnification image of the central portion of the spherulite; (B) high magnification image of white rectangular area in (A); (C) inset electron diffractogram corresponds to flat-on lamellar stacks and the arrows indicate the crystallographic *a*-axis; (D) unusual sheaflike objects.

micrographs of P[(*R*)-3HB] thin film crystallized at 60°C are shown in Fig. 2A and B. The central portion of spherulite was observed in this electron micrograph at low magnification (Fig. 2A), as with polyoxymethylene [25]. Stacked lamellar morphology was clearly observed in P[(*R*)-3HB] spherulites crystallized at 120°C, shown in Fig. 2C, and the long-axis of the lamellar crystal was parallel to the spherulite radius. Each stacking lamellar part of thin films yields a sharp electron diffraction pattern illustrated in Fig. 2C as the inset diagram. The diagram was defined by the only two orthogonal axes a^* and b^*, while the reflection originating from the crystallographic *c*-axis was not detected, indicating that the P[(*R*)-3HB] crystal forms the "flat-on" lamellae, the polymer chains align perpendicular to the lamellar base of the crystal, in the thin films and that the lamellar crystals stack parallel to the base substrate plane. From the electron diffraction pattern, it was confirmed that the long-axis of the lamellar crystals was their crystallographic *a*-axis. The lamellar width, dimension along the crystallographic *b*-axis and the crystallinity of flat-on lamellae increased with a rise in the crystallization temperature. Fig. 2C and D show the boundary region between two spherulites in a thin film crystallized at 120°C and the unusual sheaflike objects grown on the flat-on lamellar crystal surface at 120°C, respectively. The boundary between two spherulites consists of interleaved lamellae, and the amount of the interleaving depends on both the relative orientations of lamellae and the rate of nucleation. P[(*R*)-3HB] is considered as quite stiff and brittle material. The bonding weakness of interleaved lamellae among many spherulites grown by many nuclei seems to be one of the reasons for stiffness and brittleness.

Fig. 3 shows the typical electron micrographs of P[(*R*)-3HB-*co*-10 mol% 6HH] thin films. As shown in Fig. 3A, two different types of lamellar stackings can be observed in P[(*R*)-3HB-*co*-10 mol% 6HH] thin films crystallized at 50°C. One type is seen in the left side region of the micrograph, and the electron diffraction pattern exhibits the reflections characteristic of the flat-on lamellae (diffraction not shown). The other, as seen on the right side region of the micrograph, may be the "edge-on" lamellar stack although we could not obtain the electron diffractogram. The fraction of edge-on lamellae decreased with a rise in crystallization temperature, and P[(*R*)-3HB-*co*-10 mol% 6HH] thin film crystallized at 110°C was composed of only flat-on lamellae, as shown in Fig. 3B. Apparently, in the growth front of a flat-on crystal, the slight splits could be observed. This observation indicates that the rate of crystal growth is different at the micropoints in the growth front of lamellar crystal.

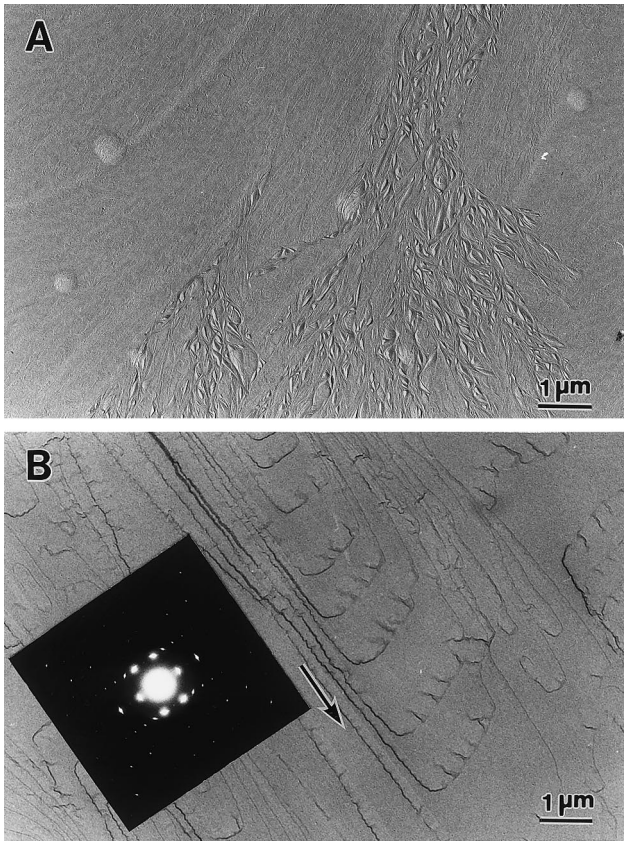

Fig. 3. Electron micrographs of P[(*R*)-3HB-*co*-10 mol% 6HH] thin films crystallized at 50°C (A) and 110°C (B). Inset: typical electron diffraction pattern corresponding to P[(*R*)-3HB-*co*-10 mol% 6HH] flat-on lamellar stacks. The arrow indicates the crystallographic *a*-axis.

The *d*-spacing values of P[(*R*)-3HB-*co*-10 mol% 6HH] lamellar crystals calculated from the electron diffractograms corresponding to flat-on lamellae were in good agreement with those values of the P[(*R*)-3HB] homopolymer. From this result we have concluded that the randomly distributed 6HH units in P[(*R*)-3HB-*co*-10 mol% 6HH] are excluded from the P[(*R*)-3HB] crystalline phase.

The features of crystalline surface for polyester thin films were further characterized by AFM. Typical AFM deflection images of P[(*R*)-3HB] thin film crystallized at 120°C on the glass substrate are shown in Fig. 4. For all samples, the flat-on lamellar stacking was detected in the images. From the height images of flat-on lamellar part in spherulites (data not shown), the lamellar periodicity was measured. The lamellar periodicities for P[(*R*)-3HB] thin film crystallized at 60 and 120°C were respectively, in the 5–7 and 8–10 nm range, and the value tended to increase with crystallization temperature. In a previous paper [17], the long period and lamellar thickness of melt-crystallized P[(*R*)-3HB] thick films (50 μm thickness) were examined by using small-angle X-ray scattering technique. The values of long period and lamellar thickness of P[(*R*)-3HB] increased from 7.4 to 12.1 nm and from 5.3 to 8.2 nm, respectively, as crystallization temperature was increased from 60 to 130°C. The values of lamellar periodicities for P[(*R*)-3HB] thin films were almost identical with the values of long period or lamellar thickness for the melt-crystallized thick films.

The striking feature of P[(*R*)-3HB] lamellar crystals was observed at the growth front of lamellae formed at relatively higher crystallization temperatures. Fig. 4B shows the higher enlargement of AFM image at the growth front regions of P[(*R*)-3HB] lamellar crystal crystallized at 120°C. At the growth front of crystalline lamellae, microfibril crystals with dimensions of 50–400 nm length, 30–50 nm width and 8–10 nm thickness were detected. Tomasi et al. [26] and Koyama and Doi [16] reported the average crystal size of P[(*R*)-3HB] crystals in the range of 23–50 nm, which were determined from X-ray diffraction of melt-crystallized P[(*R*)-3HB] films using (020) reflection. The values of average crystal size for P[(*R*)-3HB] thick films were consistent with the crystal widths of microfibril crystals in P[(*R*)-3HB] thin films. The average crystal size of P[(*R*)-3HB] crystals obtained from (020) reflection may be corresponding to the crystal width of tightly packed microfibrils in lamellar crystals.

Fig. 5 shows the AFM deflection images of P[(*R*)-3HB-*co*-10 mol% 6HH] thin film crystallized at 110°C on glass substrate. Also for P[(*R*)-3HB-*co*-10 mol% 6HH] thin film, the flat-on lamellar stacking was detected. The lamellar periodicities for P[(*R*)-3HB-*co*-10 mol% 6HH] thin film crystallized at 110°C were in the 8–10 nm range. The microfibril crystals with dimensions of 100–500 nm length, 30–50 nm width and 8–10 nm thickness were also observed significantly at the growth front of crystalline lamellae for P[(*R*)-3HB-*co*-10 mol% 6HH] thin film crystallized at 110°C (Fig. 5B).

The enzymatic hydrolysis of thin films was carried out at 37°C using 0.1 M potassium phosphate buffer (pH 7.4) containing PHB depolymerase (1.0 μg ml^{-1}) from *Alcaligenes faecalis*. Fig. 6 shows the AFM deflection images of P[(*R*)-3HB] and P[(*R*)-3HB-*co*-10 mol% 6HH] thin films after enzymatic degradation for 15 min. After enzymatic degradation lamellar crystals were degraded to smaller pieces, while the lamellar periodicities of thin films were unchanged. In addition, the ends of crystalline lamellae (*bc*-plane) acquire a jagged texture along the crystal long-axis by the function of PHB depolymerase. The projection widths (30–50 nm) of jagged texture were almost identical with the widths (30–50 nm) of microfibril crystals. Hocking et al. [18,19], Nobes et al. [20] and Iwata et al. [21,22] have performed the enzymatic degradation of single crystals with PHB depolymerases from bacteria and fungi and concluded that the attack by the active site of PHB depolymerase takes place preferentially at the crystal edges (*ac*-plane) and ends (*bc*-plane) rather than the chain-folding surfaces (*ab*-plane) of single crystals. Many narrow cracks and small crystal fragments along the crystal long-axis corresponding to the crystallographic *a*-axis were produced from P[(*R*)-3HB] single crystals by the enzymatic reaction, independent of both surface morphologies of single crystals and types of PHB depolymerases. As it is shown in Fig. 6, PHB

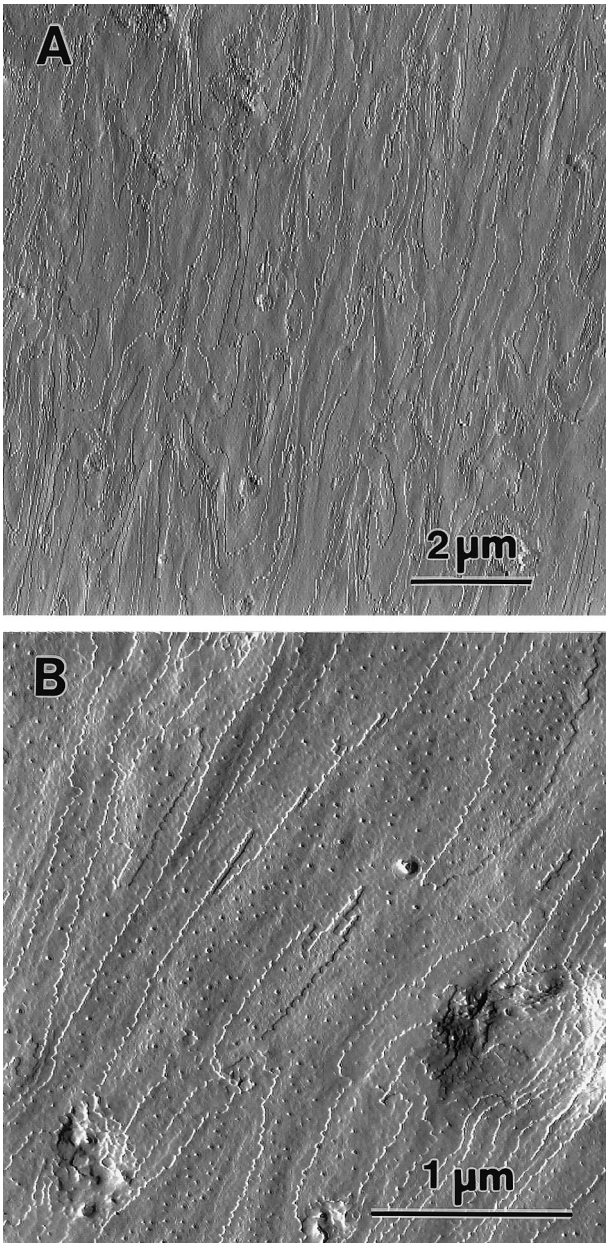

Fig. 4. AFM deflection images of P[(*R*)-3HB] thin films crystallized at 120°C (A) and higher enlargement of the AFM image (B).

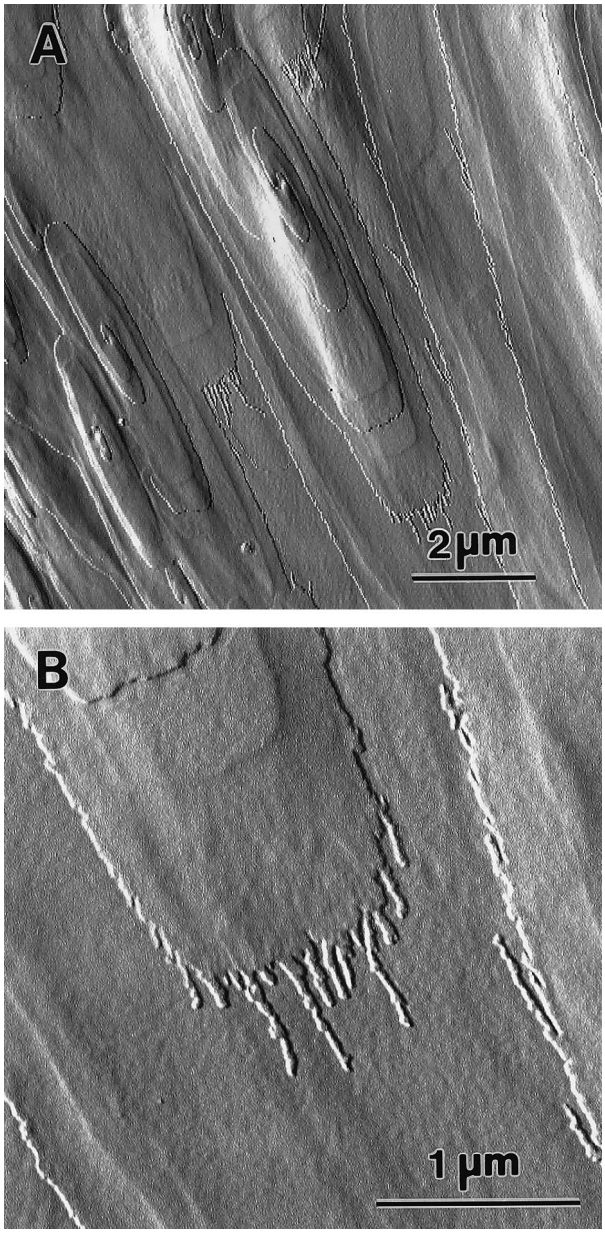

Fig. 5. AFM deflection images of P[(*R*)-3HB-*co*-10 mol% 6HH] thin films crystallized at 110°C (A) and higher enlargement of the AFM image (B).

depolymerase predominantly hydrolyze the polymer chains at the crystal edges and ends of the crystalline lamellae on the surface of thin films.

Barham et al. [12] have shown that the monolamellar single crystal of P[(*R*)-3HB] splits into smaller crystal fragments along the long-axis direction upon stretching perpendicular to its long-axis. When the single crystal was stretched parallel to its long-axis, periodic cracks intersecting the long-axis resulted. In addition, they suggested the predominant fold model in P[(*R*)-3HB] crystals along the [100] direction with existing successive folds in the [110] and [1$\bar{1}$0] directions, based on the electron micrographs of P[(*R*)-3HB] crystals decorated with polyethylene [27].

These results may suggest that the P[(*R*)-3HB] lamellar crystals consist of both tight and loose molecular packing regions and that the formation of tightly and loosely packed regions is related to the crystal growth manner for P[(*R*)-3HB]. In this study we found the presence of microfibril crystals at the growth front of lamellar crystals for both P[(*R*)-3HB] and P[(*R*)-3HB-*co*-10 mol% 6HH]. The lamellar crystals in the thin films may be the aggregate of microfibril crystals. Fig. 7 shows a schematic model on the crystal growth of P[(*R*)-3HB] lamellar crystals. In this model, we propose that the crystal growth of P[(*R*)-3HB] lamellae progresses via two steps. At first, the microfibril crystals grow from the secondary nuclei formed at growth front of

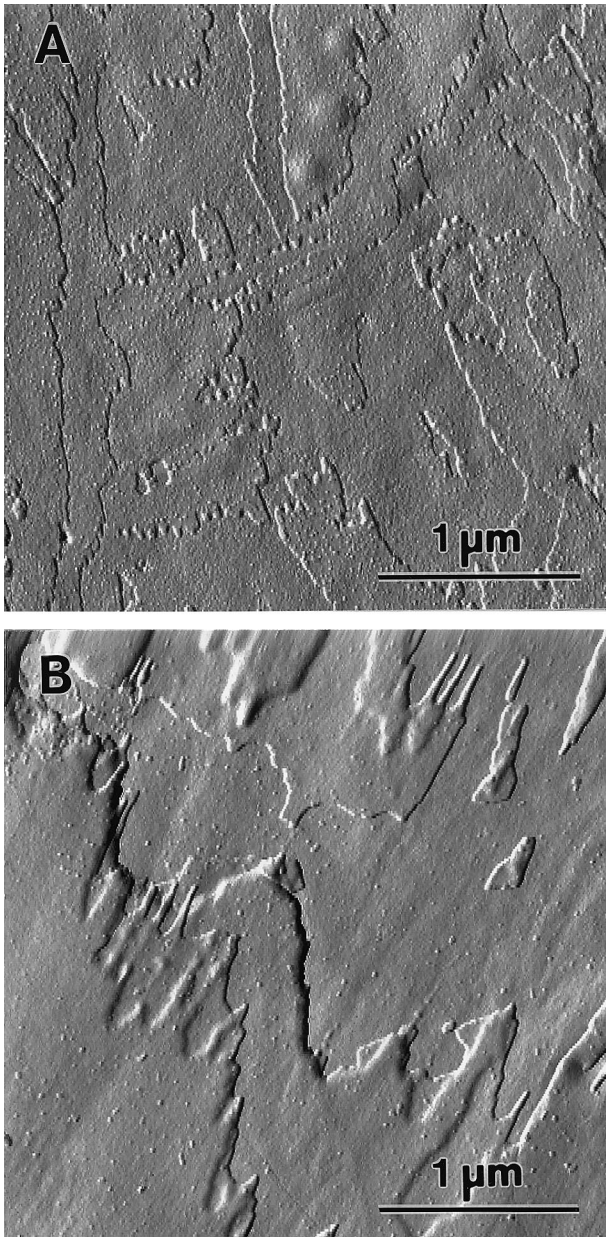

Fig. 6. AFM deflection images of thin films after enzymatic degradation by PHB depolymerase from *Alcaligenes faecalis* for 15 min. (A) P[(*R*)-3HB] thin film crystallized at 120°C; (B) P[(*R*)-3HB-*co*-10 mol% 6HH] thin film crystallized at 110°C.

lamellae. Later, residual amorphous polymer chains become incorporated into the edges of microfibril crystals or into new secondary nuclei formed at growth front to fill up the regions between the microfibril crystals. P[(*R*)-3HB] lamellar crystals propagate by the repetition of these steps. The polymer chains inside the microfibril crystals may be packed tightly. In contrast, the loose chain-packing may occur at the boundary of adjacent microfibril crystals because of limitations of the number of amorphous polymer chains and of free volume to arrange the polymer chains. The PHB depolymerase may hydrolyze predominantly the loosely packed polymer chains at the boundary of adjacent microfibril crystals and subsequently erodes tightly packed polymer chains in the microfibril crystals. Consequently, the jagged texture along the crystal long-axis may be observed at the ends of crystalline lamellae on the surface of thin films after enzymatic degradation.

The microfibril crystals were observed at the growth front of lamellae formed at higher crystallization temperatures. The rate of secondary nucleation on the growth front increases with a decrease in crystallization temperature. As a result, at lower crystallization temperatures, many microfibril crystals grow from the lamellar front and the microfibril crystal texture may hardly be detected.

A large number of investigations have been performed considering the spherulite structure, but many unsolved problems still remain about the relationship between the morphology and the growth mechanism. It is apparent that the spherulite formation is governed by at least three factors, branching of lamellar crystals, splitting of lamellae and distribution of molecular weight. However, the detailed mechanisms of branching and splitting formations in spherulitic development are not yet clear. The formation of microfibril crystals in lamellar crystals provides information to elucidate the formation of branching and splitting in lamellar crystals. For majority of common polymers whose single crystals and spherulitic morphologies have been characterized well, such as polyethylene, isotactic polystyrene, etc. the crystal growth direction is not parallel to the chain-folding direction. In contrast, the directions of chain-folding and of crystal growth are parallel in the case of P[(*R*)-3HB]. Whether or not the microfibril crystal is an inherent feature for the polymers which have parallel directions between chain-folding and crystal growth is uncertain, and needs further research.

4. Conclusions

This paper has reported the morphologies of two-dimensionally grown crystals for P[(*R*)-3HB] homopolymer and a random copolymer of 90 mol% (*R*)-3HB and 10 mol% 6HH units. From the electron diffractograms of flat-on lamellae for P[(*R*)-3HB-*co*-10 mol% 6HH], it is concluded that randomly distributed 6HH units in copolymers act as defects of P[(*R*)-3HB] crystal and are excluded from the P[(*R*)-3HB] crystalline lamellae. Microfibril crystals of 30–50 nm width are present at the growth fronts of lamellar crystals of P[(*R*)-3HB] and the copolymer, suggesting that P[(*R*)-3HB] lamellar crystals consist of microfibril crystals.

Acknowledgements

This work was supported by CREST (Core Research for Evolutional Science and Technology) of Japan Science and Technology Corporation (JST).

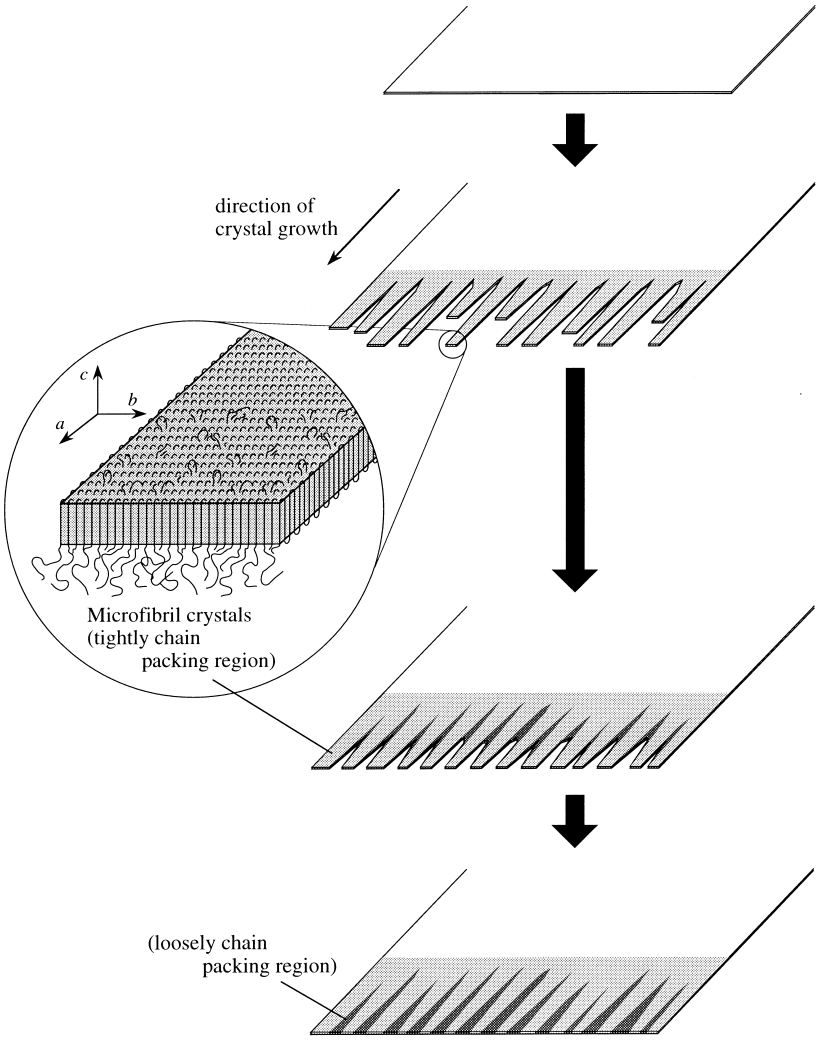

Fig. 7. Schematic model of the crystalline growth of lamellar crystals for poly(hydroxyalkanoic acids).

References

[1] Holmes PA. In: Bassett DC, editor. Developments in crystalline polymers—2, London: Elsevier, 1988. p. 1.
[2] Doi Y. Microbial polyesters, New York: VCH, 1990.
[3] Anderson AJ, Dawes EA. Microbiol Rev 1990;54:450.
[4] Tanio T, Fukui T, Shirakura Y, Saito T, Tomita K, Kaiho T, Masamune S. Eur J Biochem 1982;124:71.
[5] Mukai K, Yamada K, Doi Y. Polym Degrad Stab 1993;41:85.
[6] Jendrossek D, Schirmer A, Schlegel HG. Appl Microbiol Biotechnol 1996;46:451.
[7] Doi Y, Kanesawa Y, Kunioka M, Saito T. Macromolecules 1990;23:26.
[8] Shimamura E, Scandola M, Doi Y. Macromolecules 1994;27:4429.
[9] Doi Y, Kitamura S, Abe H. Macromolecules 1995;28:4822.
[10] Abe H, Doi Y, Aoki H, Akehata T, Hori Y, Yamaguchi A. Macromolecules 1995;28:7630.
[11] Abe H, Doi Y, Hori T, Hagiwara T. Polymer 1997;39:59.
[12] Barham PJ, Keller A, Otun EL, Holmes PJ. J Mater Sci 1984;19:2781.
[13] de Koning GJM, Scheeren AHC, Lemstra PJ, Peeters M, Reynaers H. Polymer 1994;35:4598.
[14] Kumagai Y, Kanesawa Y, Doi Y. Makromol Chem 1992;193:53.
[15] Tomasi G, Scandola M, Briese BH, Jendrossek D. Macromolecules 1996;29:507.
[16] Koyama N, Doi Y. Macromolecules 1997;30:826.
[17] Abe H, Doi Y, Aoki H, Akehata T. Macromolecules 1998;31:1791.
[18] Hocking PJ, Revol JF, Marchessault RH. Macromolecules 1996;29:2467.
[19] Hocking PJ, Marchessault RH, Timmins MR, Lenz RW, Fuller RC. Macromolecules 1996;29:2472.
[20] Nobes GAR, Marchessault RH, Chanzy H, Briese BH, Jendrossek D. Macromolecules 1996;29:8330.
[21] Iwata T, Doi Y, Kasuya K, Inoue Y. Macromolecules 1997;30:833.
[22] Iwata T, Doi Y, Tanaka T, Akehata T, Shiromo M, Teramachi S. Macromolecules 1997;30:5290.
[23] Doi Y, Tamaki A, Kunioka M, Soga K. Appl Microbiol Biotechnol 1988;28:330.
[24] Shirakura Y, Fukui T, Saito T, Okamoto Y, Narikawa T, Koide K, Tomita K, Takemasa T, Masamune S. Biochim Biophys Acta 1986;880:46.
[25] Geil PH. J Polym Sci 1960;47:65.
[26] Tomasi G, Scandola M. J Macromol Sci: Pure Appl Chem 1995;A29:671.
[27] Birley C, Briddon J, Sykes KE, Barker PA, Organ SJ, Barham PJ. J Mater Sci 1995;30:633.